Chemically Resolved Structure of the Sn/Ge(111) Surface

Tien-Lin Lee, Samantha Warren, Bruce C. C. Cowie, and Jörg Zegenhagen
European Synchrotron Radiation Facility, Boîte Postale 220, F-38043 Grenoble Cedex 9, France
(Received 15 June 2005; published 2 February 2006)

The structure and chemical states of the Sn/Ge(111) surface are characterized by x-ray standing waves combined with photoemission. For the room temperature $\sqrt{3} \times \sqrt{3}$ phase two chemical components, approximately 0.4 eV apart, are observed for both Sn 3*d* and 4*d* core levels. Our model-independent, x-ray standing wave analysis shows unambiguously that the two components originate from Sn adatoms located at two different heights separated vertically by 0.23 Å, in favor of a model composed of a fluctuating Sn layer. Contrary to the most accepted scenario, the stronger Sn 3*d* and 4*d* components, which appear at the lower binding-energy sides and account for 2/3 of the Sn adatoms, are identified to be associated with the higher Sn position, manifesting their filled valence state character.

DOI: 10.1103/PhysRevLett.96.046103 PACS numbers: 68.43.Fg, 68.49.Uv, 79.60.−i

The unusual behaviors reported for the α-Sn/Ge(111) and a few other semiconductor surfaces [1,2] have drawn broad attention in recent years. It was found that the α-Sn/Ge(111) surface undergoes a phase transition at approximately 200 K [3] between its room temperature (RT) $\sqrt{3} \times \sqrt{3}$ and low temperature (LT) 3×3 phases. Both phases have been characterized to have a metallic nature [3–5], which is often energetically unfavorable for a semiconductor surface. Although the basic structures of the α-Sn/Ge(111) surface can be well described by a simple T_4-site adsorption of 1/3 of a monolayer (ML) of Sn [6–9] [Fig. 1(a)], to establish a complete understanding of the surface has been proven to be challenging.

Theoretical [10–14] and experimental evidence [3,8,15–18] gathered by now has led us to a certain consensus that the LT 3×3 symmetry is the result of a large lattice distortion near the surface that leads to two different heights for the Sn adatoms, while energy is gained not through gap opening but largely through rehybridization involving the Sn dangling bonds and deeper Ge layers. The formation of a surface charge density wave or Mott insulator is therefore unlikely [14].

The structure of the RT $\sqrt{3} \times \sqrt{3}$ phase is, however, still under debate. An important question has been whether the Sn adatoms form a flat layer or fluctuate vertically between the two positions they occupy at LT. The former has been concluded from surface x-ray diffraction (SXRD) [8] and suggested by angle-resolved photoemission [17], while the latter is supported by core-level photoemission, which observes for the LT and RT phases the same Sn 4*d* line shape that contains two chemical components [15], as well as by photoelectron diffraction [19] and very recently by scanning tunneling microscopy (STM) [20].

Lack of precise structural information has hampered our understanding of the electronic properties of the surface. For the 3×3 phase, bias dependent STM has identified two types of Sn adatoms [3,16]. The ratio between the filled- and empty-state enhanced adatoms appears to be 1:2. While photoemission studies also indicate the presence of two chemical components for the Sn [15], the lower binding-energy 4*d* component, which in an initial-state picture is expected to originate from the more negatively charged or better valence screened Sn adatoms, is measured to be twice as strong as the higher one, in apparent contradiction to the interpretation of the STM result. To resolve this controversy, it has been argued that a large site-dependent final-state screening causes an exchange of the peak positions of the two Sn 4*d* components [11,14]. But other experiments [21,22] have shown that the intensity of the lower binding-energy 4*d* component increases upon electron doping of the surface with potassium, demonstrating the filled valence state character of its emitters.

In the present study we focus on exploring the Sn adatom structure behind the 4*d* core-level shift for the RT $\sqrt{3} \times \sqrt{3}$ phase by measuring the photoelectrons excited by an x-ray standing wave (XSW) field. Using this

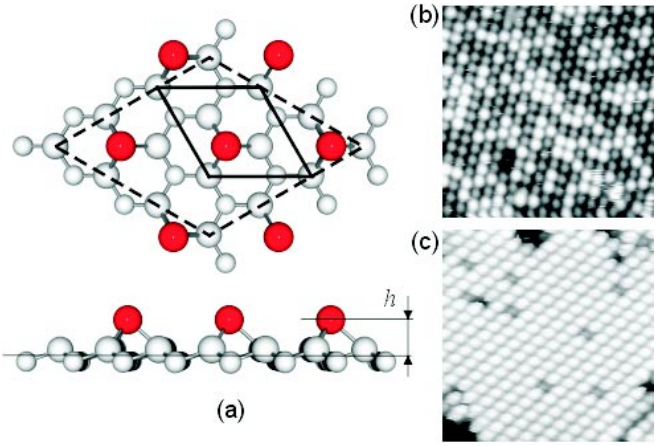

FIG. 1 (color online). Structural model for the α phase of the Sn/Ge(111) surface (a), where the solid and dashed boxes denote the $\sqrt{3} \times \sqrt{3}$ and 3×3 unit cells, respectively, and RT empty-state STM images for the (b) 2×2 (15×15 nm^2, 1.0 V and 0.1 nA) and (c) $\sqrt{3} \times \sqrt{3}$ (11×11 nm^2, 1.5 V and 0.1 nA) phases.

unique combination, which has been pioneered by Sugiyama *et al.* [23] and previously applied to probing organic adsorbate structures on metal surfaces [24], we succeeded in resolving *simultaneously* the 400 meV binding-energy shift and a 0.23 Å vertical separation of the Sn positions. Our results provide clear evidence that directly links the chemical states of the adatoms to their positions.

The experiment was carried out at beam line ID32 at the European Synchrotron Radiation Facility (ESRF). After the Ge(111) surface was cleaned by a few sputter-anneal cycles, sub-ML of Sn was evaporated from a Knudsen cell while the Ge substrate was held at approximately 350 °C. For the XSW measurements, the sample was oriented to excite the Ge(111) Bragg reflection for an incident photon energy E_γ of 2.5 keV. The XSW scans were then achieved by scanning E_γ through the Ge(111) reflection with the reflected beam intensity and core-level photoemission spectra recorded simultaneously for each E_γ. The overall energy resolution was estimated to be 500 meV.

Below 0.2 ML, STM images show that the Sn arriving at the $c(2 \times 8)$ clean surface simply substitutes the Ge adatoms in a nearly random fashion [Fig. 1(b)], leading to a 2×2 LEED pattern with diffuse, elongated spots. As the Sn coverage Θ_{Sn} increases above 0.2 ML, the more densely packed, $\sqrt{3} \times \sqrt{3}$ [Fig. 1(c)] domains appear and grow, while the 2×2 domains continue to diminish. For a surface covered only with the 2×2 structure, photoemission shows a single component in the Sn 4*d* spectrum [25]. The 2×2 surface can therefore serve as a reference in analyzing the line shape variation that accompanies the structural transition from the 2×2 to $\sqrt{3} \times \sqrt{3}$ phase [15].

Figure 2(a) shows a typical photoemission spectrum recorded from the $\sqrt{3} \times \sqrt{3}$ surface at $E_\gamma = 2.5$ keV, where the Sn 4*d* appears next to the intense Ge 3*d* peaks. A comparison of the background subtracted Sn 4*d* line shapes between the $\sqrt{3} \times \sqrt{3}$ ($\Theta_{\mathrm{Sn}} = 0.33$ ML) and 2×2 ($\Theta_{\mathrm{Sn}} = 0.2$ ML) phases is presented in Fig. 2(b). The broadening of the peaks is clearly visible and thus confirms the presence of a second component for the $\sqrt{3} \times \sqrt{3}$ phase. Consistent with most published results, the peak shape exhibits asymmetry for the $\sqrt{3} \times \sqrt{3}$ phase with the maximum of each spin-orbital component shifting towards the lower binding-energy side, indicating that the majority of the Sn (component 1) has a lower binding energy than the minority (component 2).

In addition to confirming the peak width broadening, the comparison with the 2×2 core levels also offers a reliable way for quantitative line-shape analysis on the more complicated $\sqrt{3} \times \sqrt{3}$ spectra. Here we describe each photoemission line with the convolution of a Gaussian and a Lorentzian function. By first fitting the 2×2 spectra, we extract the peak width, spin-orbital split, and branching ratio for the Sn 4*d* peaks. We then analyze the line shapes for the $\sqrt{3} \times \sqrt{3}$ phase by fixing these values and allowing only the energy separation ΔE_B between the two chemical components and their intensity ratio I_1/I_2 to vary. We determine this way $\Delta E_B = 410$ meV and $I_1/I_2 = 1.9$, in good agreement with the reported values [16].

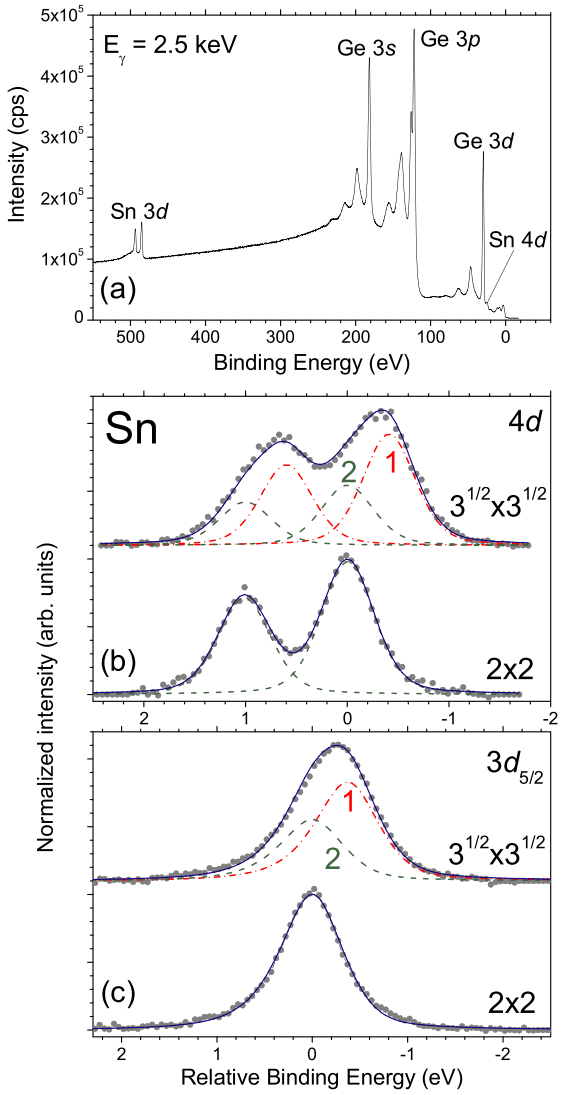

FIG. 2 (color online). Off-Bragg survey scan of the photoemission spectrum for the $\sqrt{3} \times \sqrt{3}$ surface (a), and comparison of the line shapes between the $\sqrt{3} \times \sqrt{3}$ and 2×2 phases for the Sn 4*d* (b) and $3d_{5/2}$ (c) core levels.

Having verified the presence of the two distinct Sn species for the $\sqrt{3} \times \sqrt{3}$ phase, we probe their sites by scanning the standing wave field generated by the substrate (111) reflection across the Sn layer. In this way, we determine the vertical positions of the Sn adatoms with respect to the substrate lattice.

Figure 3(a) shows the background removed Sn 4*d* spectra recorded at six different incident energies over 1.5 eV centered around the Ge(111) Bragg peak. As E_γ increases, the 180° phase shift between the incident and diffracted x-rays causes the XSW antinodes to move along the $(\bar{1}\,\bar{1}\,\bar{1})$ direction by one half of the XSW period and thus modulates the photoelectron yields [26]. If the two Sn 4*d* com-

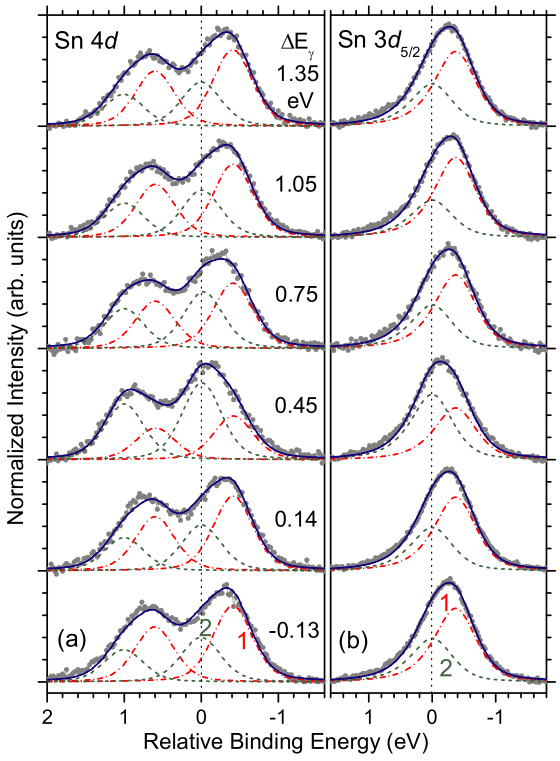

FIG. 3 (color online). XSW-modulated Sn 4d (a) and 3d (b) spectra recorded at six incident energies centered around the Ge(111) reflection and best fits with the two components deduced from Figs. 2(b) and 2(c). All spectra are normalized to their peak heights.

ponents are associated with different heights, the line shape may vary as a function of E_γ as well. To highlight any line-shape variation, the spectra in Fig. 3(a) have been divided by their peak heights. After such normalization the data already reveal, as E_γ approaches the center of the Ge(111) reflection, a continuous shift of the peak maxima of both spin-orbital components towards the high binding-energy side, which reaches its maximum at $\Delta E_\gamma = 0.45$ eV. Further line-shape analysis based on the 4d peak shape deduced from Fig. 2(b) and allowing only I_1 and I_2 to vary shows more convincingly that the intensity ratio I_1/I_2 deviates from its off-Bragg value to a nearly complete inversion of the ratio at $\Delta E_\gamma = 0.45$ eV. This XSW induced line-shape variation provides clear evidence that directly links the two Sn 4d components to two different sites above the Ge(111) surface.

To quantify the structural differences between the two components, we carried out a full XSW analysis on the modulated peak intensities for the core levels. For a Bragg reflection $\mathbf{H}$, the photoelectron yield induced by the interference field can be described as a function of E_γ as [26]

$$Y(E_\gamma) = Y_{\mathrm{OB}}\{1 + R(E_\gamma) + 2\sqrt{R(E_\gamma)} f_{\mathbf{H}} \cos[\nu(E_\gamma) - 2\pi P_{\mathbf{H}}]\}, \quad (1)$$

where R is the reflectivity, Y_{OB} the yield at $R = 0$, and ν the phase of the standing waves. The coherent fraction ($f_{\mathbf{H}}$) and coherent position ($P_{\mathbf{H}}$) measure essentially the width and center, respectively, of a atomic distribution projected onto the $\mathbf{H}$ direction. With R and ν evaluated from the dynamical diffraction theory, Y_{OB}, $f_{\mathbf{H}}$, and $P_{\mathbf{H}}$ can be directly determined by a least-squares fit.

Figure 4(a) depicts the best fits of Eq. (1) to the integrated Sn 4d peak intensities for components 1, 2, and their sum, which have been rescaled such that $Y_{\mathrm{OB},1} + Y_{\mathrm{OB},2} = 3.0$. The deduced $f_{\mathbf{111}}$ and $P_{\mathbf{111}}$ are listed in Table I, where h is the height above the topmost bulk-extrapolated Ge(111) plane [Fig. 1(a)] and is equal to $P_{\mathbf{111}}$ multiplied by the spacing of the Ge(111) lattice planes (3.26 Å). The results of our XSW analysis reveal unambiguously that it is the lower binding-energy component, or component 1, that is associated with the higher Sn. The vertical separation between the two Sn positions (Δh) is found to be 0.23 Å, in good agreement with theoretical calculations [14]. The populations determined by Y_{OB} also yields a ratio virtually equal to 2.0 between component 1 and 2.

Since the lifetime width of a Sn 3d core hole (~400 meV, [27]) is comparable to the energy separation between the above two 4d components, a shift in binding energy should also be observed in the Sn 3d spectrum. This is clearly demonstrated by the peak broadening in Fig. 2(c), where we explore the line-shape differ-

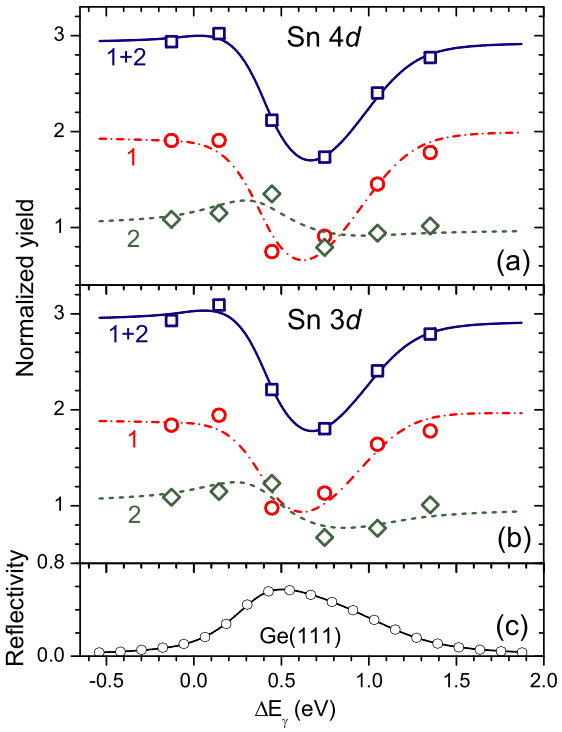

FIG. 4 (color online). Best fits of Eq. (1) to the normalized peak intensities I_1, I_2, and $I_1 + I_2$ for the Sn (a) 4d and (b) 3d core levels (see text). (c) Measured and calculated Ge(111) reflectivity curves.

TABLE I. Structural parameters for the Sn adatoms deduced from the present 4*d* and 3*d* XSW analysis for the $\sqrt{3} \times \sqrt{3}$ phase.

	Comp.	f_{111}	P_{111}	$Y_{OB,1}/Y_{OB,2}$	h (Å)	Δh (Å)
4*d*	1	0.86	0.80		2.61	
	2	0.40	0.73	1.96	2.38	0.23
	1 + 2	0.68	0.79		2.58	
3*d*	1	0.75	0.80		2.61	
	2	0.52	0.73	1.92	2.38	0.23
	1 + 2	0.66	0.78		2.55	

ence of the Sn $3d_{5/2}$ peak between the 2×2 and $\sqrt{3} \times \sqrt{3}$ phases. Assuming two components in the analysis, the 3*d* line shape for the $\sqrt{3} \times \sqrt{3}$ phase can be best reproduced by $\Delta E_B = 370$ meV and $I_1/I_2 = 1.8$. When excited by the Ge(111) XSW field [Fig. 3(b)], the 3*d* intensity modulations closely resemble the 4*d* case, as marked by the common behavior that I_2 surpasses I_1 at $\Delta E_\gamma = 0.45$ eV. Further comparison of the integrated 3*d* peak intensities with Eq. (1), as summarized in Fig. 4(b) and Table I, confirms the above 4*d* XSW analysis.

To explain the different observations between STM and core-level photoemission, which indicate one and two, respectively, Sn species for the $\sqrt{3} \times \sqrt{3}$ surface, it has been proposed [15] that the RT phase contains a buckled Sn layer with the adatoms fluctuating vertically between the two equilibrium 3×3 positions. Recent molecular dynamics simulations [15,28] further suggest that, in addition to the classical, temperature-driven lattice vibration around each of the two 3×3 sites, the $\sqrt{3} \times \sqrt{3}$ structure can be realized by an electronically driven, instantaneous switching at a high frequency of the Sn adatoms between the two sites. This tunneling nature of the fluctuations, together with the comparably fast photoemission process, as outlined by the Frank-Condon principle, permits a straightforward interpretation of our XSW results: The different heights associated with the two Sn core-level components represent the two temporarily occupied sites of the Sn adatoms in the RT $\sqrt{3} \times \sqrt{3}$ structure. It is also interesting to notice that the measured f_{111} values in Table I appear lower for the lower Sn.

Several local density approximation calculations [11–14] have pointed out the role of the interaction between the Sn dangling bond states and the orbitals of the four underlying Ge atoms in minimizing the energy of the surface. It is found that the filling of a dangling bond weakens the Sn-Ge bonds underneath and lifts the Sn. This theoretical prediction implies, as compared with the present result, that the lower binding-energy Sn 4*d* component corresponds indeed to those Sn adatoms with a more filled nature in their dangling bond states. This tendency is supported by the charge-impurity induced Sn 4*d* line-shape variation reported in Refs. [21,22], and is consistent with the interpretation of a core-level binding-energy shift considering predominantly the initial-state effects in the photoemission process. Structurally, this "two up and one down" configuration we found for the Sn adatoms has also been suggested by a more recent SXRD analysis [29] based on an extended data set. Note that since all core-level photoemission studies have so far detected no obvious differences in the 4*d* line shapes between the RT and LT phases, our results should also hold for the LT phase.

To conclude, the structure responsible for the Sn core-level shifts observed for the α phase of the Sn/Ge(111) surface was determined by XSWs and photoemission. Our analysis for the $\sqrt{3} \times \sqrt{3}$ phase unveils direct evidence that links the two Sn core-level components with two different heights separated by 0.23 Å. In addition, we show unambiguously that the lower binding-energy component is associated with the higher Sn.

We would like to thank R. Feidenhans'l, O. Bunk, M. J. Bedzyk, R. G. Jones, and D. P. Woodruff for helpful discussions.

[1] J. M. Carpinelli *et al.*, Nature (London) **381**, 398 (1996).
[2] H. W. Yeom *et al.*, Phys. Rev. Lett. **82**, 4898 (1999).
[3] J. M. Carpinelli *et al.*, Phys. Rev. Lett. **79**, 2859 (1997).
[4] A. Goldoni and S. Modesti, Phys. Rev. Lett. **79**, 3266 (1997).
[5] J. Avila *et al.*, Surf. Sci. **433–435**, 327 (1999).
[6] J. S. Pedersen *et al.*, Surf. Sci. **189**, 1047 (1987).
[7] M. Gothelid *et al.*, Surf. Sci. **271**, L357 (1992).
[8] O. Bunk *et al.*, Phys. Rev. Lett. **83**, 2226 (1999).
[9] J. S. Okasinski *et al.*, Phys. Rev. B **69**, 041401 (2004).
[10] G. Santoro *et al.*, Phys. Rev. B **59**, 1891 (1999).
[11] R. Stumpf *et al.*, Phys. Rev. B **59**, 15 779 (1999).
[12] S. de Gironcoli *et al.*, Surf. Sci. **454–456**, 172 (2000).
[13] R. Perez *et al.*, Phys. Rev. Lett. **86**, 4891 (2001).
[14] G. Ballabio, Phys. Rev. Lett. **89**, 126803 (2002).
[15] J. Avila *et al.*, Phys. Rev. Lett. **82**, 442 (1999).
[16] A. V. Melechko *et al.*, Phys. Rev. B **61**, 2235 (2000).
[17] T. E. Kidd *et al.*, Phys. Rev. Lett. **85**, 3684 (2000).
[18] L. Petaccia *et al.*, Phys. Rev. B **63**, 115406 (2001).
[19] L. Petaccia *et al.*, Phys. Rev. B **64**, 193410 (2001).
[20] F. Ronci *et al.*, Phys. Rev. Lett. **95**, 156101 (2005).
[21] M. Goshtasbi Rad *et al.*, Surf. Sci. **477**, 227 (2001).
[22] M. E. Dávila *et al.*, Phys. Rev. B **70**, 241308(R) (2004).
[23] M. Sugiyama *et al.*, Phys. Rev. B **51**, 14 778 (1995).
[24] G. J. Jackson *et al.*, Phys. Rev. Lett. **84**, 119 (2000).
[25] R. I. G. Uhrberg *et al.*, Phys. Rev. Lett. **85**, 1036 (2000).
[26] J. Zegenhagen, Surf. Sci. Rep. **18**, 199 (1993).
[27] M. Ohno and G. van Riessen, J. Electron Spectrosc. Relat. Phenom. **128**, 1 (2003).
[28] D. Farias *et al.*, Phys. Rev. Lett. **91**, 016103 (2003).
[29] J. Avila *et al.* (private communication).